Microscopy and Microanalysis, page 1 of 4
doi:10.1017/S1431927618000442

Microscopy AND Microanalysis

Original Article

Methods for Conducting Electron Backscattered Diffraction (EBSD) on Polycrystalline Organic Molecular Thin Films

Kevin Abbasi[1], Danqi Wang[1], Michael A. Fusella[2], Barry P. Rand[2,3] and Amir Avishai[1]

[1]Swagelok Center for Surface Analysis of Materials, Case School of Engineering, Case Western Reserve University, Cleveland, OH 44106, USA, [2]Department of Electrical Engineering, Princeton University, Princeton, NJ 08544, USA and [3]Andlinger Center for Energy and the Environment, Princeton University, Princeton, NJ 08544, USA

Abstract

Electron backscattered diffraction (EBSD) is a technique regularly used to obtain crystallographic information from inorganic samples. When EBSD is acquired simultaneously with emitting diodes data, a sample can be thoroughly characterized both structurally and compositionally. For organic materials, coherent Kikuchi patterns do form when the electron beam interacts with crystalline material. However, such patterns tend to be weak due to the low average atomic number of organic materials. This is compounded by the fact that the patterns fade quickly and disappear completely once a critical electron dose is exceeded, inhibiting successful collection of EBSD maps from them. In this study, a new approach is presented that allows successful collection of EBSD maps from organic materials, here the extreme example of a hydrocarbon organic molecular thin film, and opens new avenues of characterization for crystalline organic materials.

Key words: electron backscattered diffraction, EBSD, orientation mapping, SEM, organic semiconductor thin film

(Received 27 February 2018; revised 13 April 2018; accepted 5 May 2018)

Introduction

Electron backscattered diffraction (EBSD) is a powerful technique widely used for crystal orientation determination in scanning electron microscopy (SEM) (Britton et al., 2016). When diffraction is obtained in the spot mode (the regular SEM imaging mode with a stationary focused electron beam), crystal orientation of the volume under the beam can be derived. Such diffraction comes from a few 10 s of nanometers depth. For modern field-emission SEMs, spatial resolution (in the *xy* plane) well below 100 nm can be routinely achieved (Avishai et al., 2015). Therefore, polycrystalline samples can be mapped to study crystal orientation by rastering the electron beam on sample surfaces while collecting corresponding EBSD patterns.

Even though EBSD is widely used to study inorganic materials, e.g. metals and ceramics, it is very difficult to study organic materials due to the sensitivity of their structure to the beam. Once an electron beam is focused on an organic sample, local sample heating will occur, which rapidly causes deterioration of the crystallinity of the sample. Therefore, although coherent EBSD patterns do initially appear on the detector, they quickly fade and eventually disappear. Such damage is permanent and eliminates the possibility of acquiring subsequent diffraction on that same spot. Strategies to reduce the electron damage using a defocused beam has been utilized for the analysis of sodium in glass (Morgan & London, 1996). Quantitative electron beam damage on different organic thin films has been studied and it has been shown that different films have different critical electron doses (per unit area) that, if exceeded, result in the deterioration of the electron diffraction (Leijten et al., 2017). This paper presents two different experimental approaches to address and overcome this difficulty.

Tetraphenyltetracene, or rubrene, is a promising organic semiconductor due to its demonstrated high field-effect transistor mobilities (Jurchescu et al., 2006). Its major potential applications are in organic light emitting diodes (OLEDS) and field-effect transistors, which are the core elements for flexible displays. Single crystal transistors can be prepared by using crystalline rubrene, often grown in a modified zone furnace with a temperature gradient (Jurchescu et al., 2006). Rubrene is a hydrocarbon, with chemical formula $C_{42}H_{28}$ (Jurchescu et al., 2006).

Polycrystalline rubrene takes at least three distinct crystal structures (Taylor, 1936; Henn et al., 1971; Jurchescu et al., 2006). In this study, we investigate rubrene thin films adopting the orthorhombic structure, space group Cmca. Its unit cell dimensions are $a = 2.68$ nm, $b = 0.71$ nm, and $c = 1.44$ nm (Henn et al., 1971; Jurchescu et al., 2006).

Experimental Details

Polycrystalline rubrene thin films were grown on a glass slide coated with a layer of indium tin oxide using a post-deposition annealing method to thermally convert a ~20 nm thick as-deposited amorphous rubrene thin film into a crystalline thin film (Fusella et al., 2017*b*). Depositing an additional 80 nm of rubrene atop this crystalline template has been shown to propagate the crystallinity and yield a net 100 nm thick polycrystalline rubrene film (Fusella et al., 2017*a*). Imaging with polarized transmission

Author for correspondence: Kevin Abbasi, E-mail: kevin.abbasi@case.edu

Cite this article: Abbasi K, Wang D, Fusella MA, Rand BP, Avishai A (2018) Methods for Conducting Electron Backscattered Diffraction (EBSD) on Polycrystalline Organic Molecular Thin Films. *Microsc Microanal*. doi: 10.1017/S1431927618000442

optical microscopy shows that the rubrene thin film contains polycrystalline grains with an average size of ~150 μm (Fig. 1). In addition, previous X-ray diffraction studies have shown these films to be strongly textured with the {100} poles parallel to the growth direction (growth along the axis of the crystal). The sample preparation procedure along with film characterizations were previously studied in detail (Fusella et al., 2017*a*, 2017*b*).

A FEI Nova Nanolab 200 FEG-SEM (Hillsboro, OR, USA) was used to investigate the film microstructure. The microscope is equipped with an Oxford Nordlys Nano EBSD (Abingdon, Oxfordshire, UK) detector with forward scattered detectors.

The following acquisition parameters were surveyed to optimize Kikuchi diffraction pattern quality. The acceleration voltage was varied between 2 and 20 kV, beam current between 500 pA to a few nA and detector exposure time varied in the range of 10–500 ms. Different combinations of probe current and acquisition time led to a rapid disappearance of the Kikuchi patterns on the detector. To overcome this difficulty, the following two approaches were developed.

(1) *Window technique*: acquisition of a Kikuchi pattern using a reduced area window within the boundaries of a single domain, together with a fast rastering of a focused beam/image. Dwell times (amount of time per acquisition pixel) of 50–100 ns were used, compared with 10–30 μs normally used for imaging. Only the usage of a 4×4 detector binning was successful. The beam was rastered in a reduced area of 20×20 μm or 30×30 μm. This significantly decreases the electron dose on the sample.

(2) *Defocusing technique*: this technique was inspired by the window technique as a way to obtain a full orientation map rather than only a point pattern. Since the experimental EBSD setup does not allow setting a raster area as an acquisition point for mapping, using a defocused beam served as an alternative method to reduce the electron dose. Defocusing the electron beam effectively changes the focal point of the beam from the sample surface to the point that is above or below the surface, thereby forming a disc on the actual surface of the sample (actually an ellipse for a tilted sample).

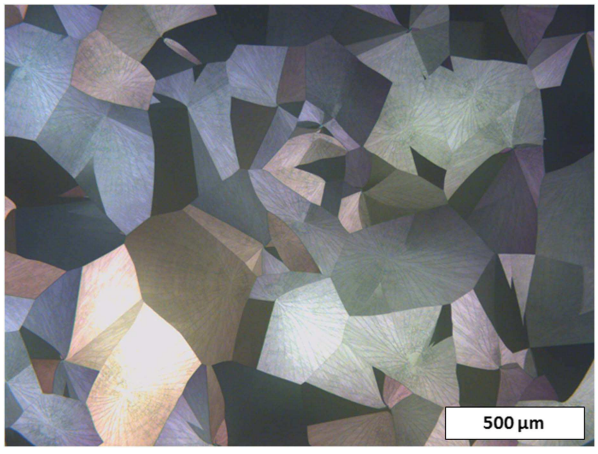

Figure 1. Polarized optical microscope image shows a polycrystalline structure with an average grain size of approximately 500 µm.

Results and Discussion

This paper's focus is to define a balance between the pattern's signal to noise ratio and step size required to generate an orientation map. The first parameter to determine is the minimum dose threshold (current and time per unit area) to collect a good quality pattern. This is followed up by the maximum dose threshold that will avoid sample damage. A successful combination of the dose threshold will be used to define the step size of the orientation map. Kikuchi patterns captured via the window technique originate from the entire area within the window. As long as the window is selected within a single crystal domain, i.e. no change of orientation, then the recorded pattern is sharp and if the window is large enough the electron dose is no longer a constraint (since patterns completely overlap and the beam does not dwell on the same spot for a significant period of time).

Figure 2 shows EBSD patterns acquired from several regions in two adjacent grains in the film. Without further processing, raw EBSD patterns show a unique orientation in each grain. A slight rotation around the axis is observed between the two grains (as evidenced by the movement of the pole in the patterns between the two grains). This mode gives accurate orientation information of the film; however, it is not possible to get an orientation map from the area.

Figure 3 shows an orientation map that was successfully acquired via the defocusing technique. This "regular" EBSD map was acquired by defocusing the beam by 2 mm with a step size of

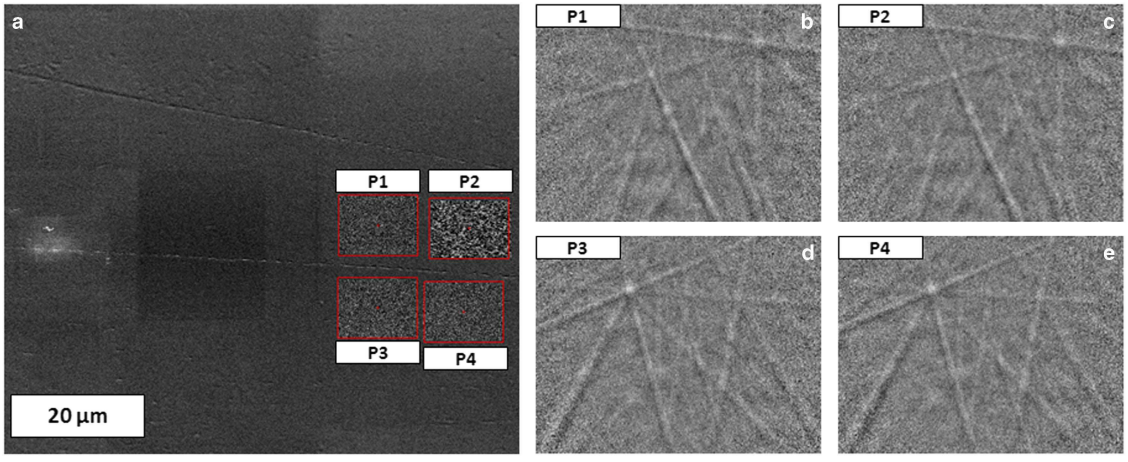

Figure 2. **a**: Secondary electron image of the film. **b**–**e**: Electron backscattered diffraction patterns obtained from areas in two adjacent grains as delineated in (**a**).

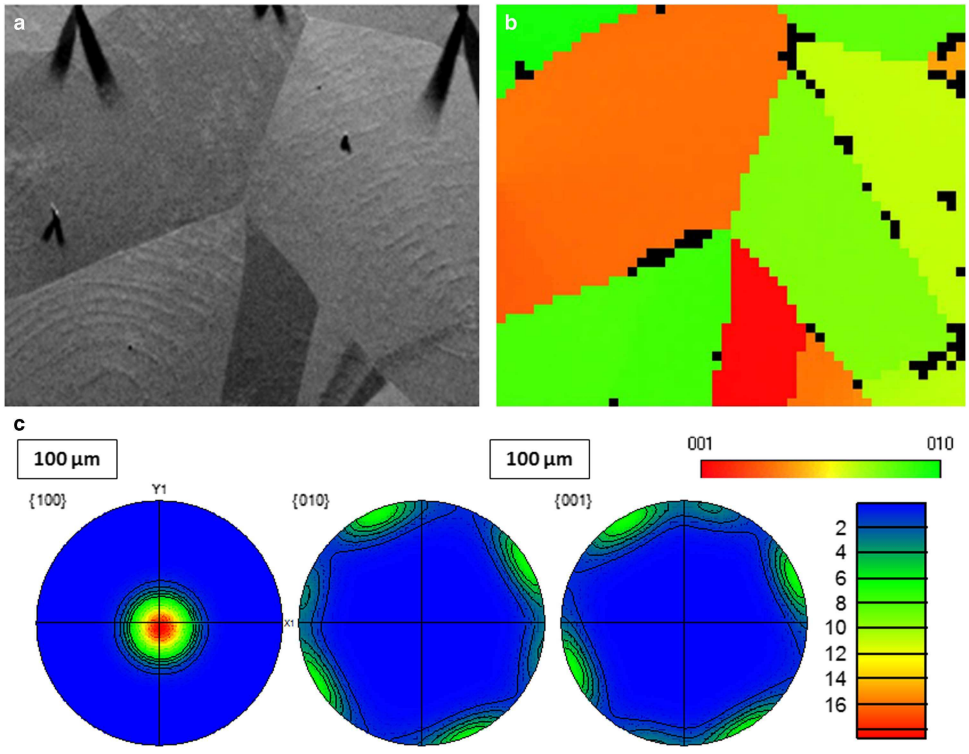

Figure 3. **a**: Forward scattered detector image and (**b**) corresponding orientation map (inverse pole figure – X) of the same region. **c**: Pole figures of the orientations obtained from the map shown in (**b**). The pole figures are showing that the rubrene film is highly textured.

10 μm, beam at 10 kV and 3.7 nA, and 480 ms detector exposure time per step. It should be noted that the working distance, as well as the size of the final aperture will influence the electron beam convergence angle and therefore determine the defocus value needed to obtain the desired beam diameter. The orientation map obtained resembles typical EBSD maps of inorganic materials, with the similar issue that pixels located near grain boundaries cannot be indexed due to pattern overlap. Overall, the index rate is well above 90%. The rubrene film is highly textured which is confirmed by the pole figure (Fig. 3c), which is complimentary to the XRD results. This confirms the *c*-axis is out of plane with a random distribution (no texturing) based on rotations of the orthorhombic structure around the *c*-axis.

By defocusing the electron beam by 2 mm, we effectively obtained an analyzed area equivalent to the window method approach but were still able to take advantage of the automated control of the EBSD system. Moreover, after obtaining a full EBSD map, all conventional tools used for post data analysis are available (Tango, Mambo software from Oxford).

The essential objective for the two techniques is the same: reducing the accumulated electron dose per unit area and time. The window approach is more suitable for the initial stage of exploring the approximate conditions needed to acquire the EBSD patterns, while the defocusing approach is necessary to collect a full map. In order to obtain the previous orientation map, an SEM image of the region to be analyzed was acquired with a focused electron beam and then the beam was defocused to optimize EBSD map acquisition.

Setting the optimal parameters is crucial to successful EBSD acquisitions. Various beam acceleration voltages were tested, and acquisitions carried out with accelerating voltages above 20 kV were not successful. Rapid degradation of the pattern quality was observed, no matter what beam current was selected. Similarly, higher primary beam currents tend to damage the sample quickly. Initially, decent quality EBSD patterns could be collected on the detector. However, with longer acquisition time needed for a better signal to noise ratio, the patterns degrade. In addition, decreasing beam currents to 1 nA or lower requires even longer exposure times to obtain decent patterns. Balancing the signal to noise ratio by altering the dwell time and current was unsuccessful, since the overall dose needed always exceeds the tolerance of the material.

As the dwell time increases, the electron dosage increases per pixel at any given time and so does the beam damage, which ultimately deteriorates the crystal. Therefore, the approach used in the two methods simply increased the interaction volume and by doing so, reduced the electron dose per unit area to a level below the degradation threshold.

Setting the beam defocus properly is another important parameter for successful data acquisition. In order to establish the necessary defocus, beam contamination points, similar to the one shown in Figure 4c, were used to estimate the convergence angle at the working conditions. These calculations indicated a convergence angle value of 5 mrad. Under these conditions, by assuming a point disc at the focus height, a 2 mm defocus results in a 10 μm disc at the sample surface (Fig. 4). Due to the high tilt angle, the radiated area is about 10×30 μm. Given the large grain size in the film, such a beam size is sufficient to resolve the film microstructure. To approximate a limit for the accumulated electron dose for this type of sample, with the same defocusing and acceleration voltage, successful acquisitions were acquired with detector exposure times of 24 and 48 ms with beam current of 3.7 and 0.9 nA, respectively. Beam currents above 3.7 nA did not result in successful patterns. Other possible parameters, e.g. T_g of the material, will be discussed later in detail in another paper.

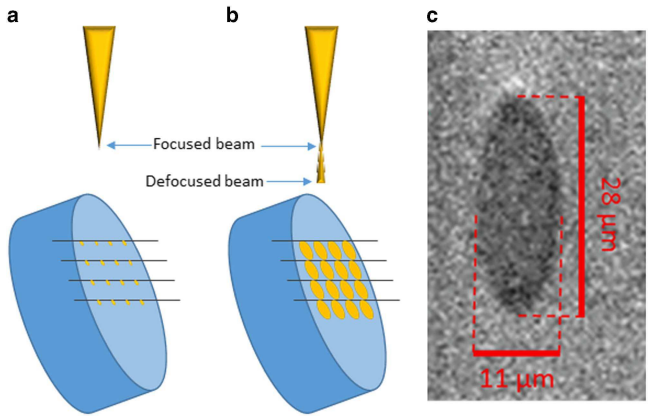

Figure 4. Illustration of electron beam projection on a tilted specimen surface when focused (**a**) compared to defocused (**b**). Secondary electron image of an actual electron beam contamination resulting from spot mode acquired at 10 kV, 3.7 nA with a 70° tilt.

It is important to mention that alternative techniques are reported to minimize beam damage during EBSD analysis such as using a cryo-stage for ice crystals (Weikusat et al., 2011). However, this demands a specialized setup. Another important recent development is the introduction of new EBSD detector technologies using CMOS sensors. The high speed and improved sensitivity both reduce the requirement for beam defocusing and therefore increase the resolution and speed of pattern collection of organic molecular thin films.

Conclusion

To the best of our knowledge, this is the first time a full orientation map was successfully obtained in the SEM for an organic material, here using an example of a polycrystalline hydrocarbon thin film. The key parameters identified in this paper for successful acquisition, and which were determined empirically, are the minimal electron dose per unit area needed for a resolvable pattern. This method enables a more in-depth study of the crystal orientation of organic materials adding to well-established methods developed over decades of research on inorganic materials.

Acknowledgments. B.P.R. and M.A.F. acknowledge funding from the National Science Foundation, award no. ECCS-1709222, and the U.S. Department of Energy, Office of Basic Energy Sciences, Division of Materials Science and Engineering under award no. DE-SC0012458. The authors would like to acknowledge the help of Scott Sitzman from Oxford Instruments and Arthur Heuer from Case Western Reserve University for useful discussions.

References

Avishai A, Abbasi K, Wang D, Avishai N, Wu D, Bedekar V, Hyde S, Sitzman S and Heuer A (2015) Tackling characterization challenges in high deformation/stress steel alloys using transmission Kikuchi diffraction (TKD). *Microsc Microanal* **21**, 2377–2378.

Britton TB, Jiang J, Guo Y, Vilalta-Clemente A, Wallis D, Hansen LN, Winkelmann A and Wilkinson AJ (2016) Tutorial: crystal orientations and EBSD – Or which way is up? *Mater Charact* **117**, 113–126.

Fusella MA, Schreiber F, Abbasi K, Kim JJ, Briseno AL and Rand BP (2017a) Homoepitaxy of crystalline rubrene thin films. *Nano Lett* **17**, 3040–3046.

Fusella MA, Yang S, Abbasi K, Choi HH, Yao Z, Podzorov V, Avishai A and Rand BP (2017b) Use of an underlayer for large area crystallization of rubrene thin films. *Chem Mater* **29**, 6666–6673.

Henn DE, Williams WG and Gibbons DJ (1971) Crystallographic data for an orthorhombic form of rubrene. *J Appl Crystallogr* **4**, 256.

Jurchescu OD, Meetsma A and Palstra TTM (2006) Low-temperature structure of rubrene single crystals grown by vapor transport. *Acta Crystallogr B Struct Sci* **62**, 330–334.

Leijten ZJWA, Keizer ADA, de With G and Friedrich H (2017) Quantitative analysis of electron beam damage in organic thin films. *J Phys Chem C* **121**, 10552–10561.

Morgan G and London D (1996) Optimizing the electron microprobe analysis of hydrous alkali aluminosilicate glasses. *Am Mineral* **81**, 1176–1185.

Taylor WH (1936) X-ray measurements on diflavylene, rubrene, and related compounds. *Z Kristallog Cryst Mater* **93**, 151–155.

Weikusat I, De Winter DAM, Pennock GM, Hayles M, Schneijdenberg CTWM and Drury MR (2011) Cryogenic EBSD on ice: Preserving a stable surface in a low pressure SEM. *J Microsc* **242**, 295–310.